additional cysteine S-H group. To address further the impact of coordination number on the ability to cleave the Hg-C bond, we examined the corresponding reactivity of strictly two-coordinate mercury-alkyl compounds that bear a close relationship to [κ^1-Tm$^{Bu^t}$]HgR. Specifically, we investigated the 1-*t*-butylimidazole-2-thione derivatives {[Hmim$^{Bu^t}$]HgR}$^+$ (*37*) in which the Hmim$^{Bu^t}$ ligand emulates the κ^1 coordination mode of the [Tm$^{Bu^t}$] ligand, as determined by x-ray diffraction studies on {[Hmim$^{Bu^t}$]HgEt}[BF_4] (*38*, *39*).

Interestingly, whereas [Tm$^{Bu^t}$]HgMe and [Tm$^{Bu^t}$]HgEt react rapidly with PhSH at room temperature, the two-coordinate compounds {[Hmim$^{Bu^t}$]HgMe}$^+$ and {[Hmim$^{Bu^t}$]HgEt}$^+$ are stable under comparable conditions; protolytic cleavage and liberation of RH are nonetheless observed at elevated temperatures (Scheme 3) (*40*). The lower reactivity of {[Hmim$^{Bu^t}$]HgR}$^+$ relative to [Tm$^{Bu^t}$]HgR supports the proposal that access to coordination numbers greater than 2 promotes protolytic cleavage of the Hg-C bond (*41*). In support of this suggestion, addition of Hmim$^{Bu^t}$ to a mixture of {[Hmim$^{Bu^t}$]HgEt}[BF_4] and PhSH causes elimination of ethane at room temperature, an observation consistent with the formation of a higher-coordinate species {[Hmim$^{Bu^t}$]$_n$HgEt}$^+$ that is more susceptible to Hg-C protolytic cleavage than is two-coordinate {[Hmim$^{Bu^t}$]HgEt}$^+$ (*42*).

In view of the low reactivity of two-coordinate {[Hmim$^{Bu^t}$]HgR}$^+$ toward PhSH, we attribute the high reactivity of [Tm$^{Bu^t}$]HgMe and [Tm$^{Bu^t}$]HgEt to the accessibility of a higher-coordinate mercury alkyl by κ^2 or κ^3 binding of the [Tm$^{Bu^t}$] ligand. Thus, of the three nonstructural cysteine residues of *MerB* that are crucial for enzymatic activity, it is evident that one cysteine is required to coordinate [HgR]$^+$ in a linear manner, a second cysteine is required to activate the Hg-alkyl group toward protolytic cleavage, and the third cysteine is required to effect the cleavage reaction (*43*, *44*).

References and Notes

1. T. W. Clarkson, L. Magos, *Crit. Rev. Toxicol.* **36**, 609 (2006).
2. H. C. Tai, C. Lim, *J. Phys. Chem. A* **110**, 452 (2006).
3. A. Hartwig *et al.*, *Food Chem. Toxicol.* **40**, 1179 (2002).
4. For other examples of Hg(II) binding to zinc finger proteins, see (*5*, *6*).
5. M. Razmiafshari, J. Kao, A. d'Avignon, N. H. Zawia, *Toxicol. Appl. Pharmacol.* **172**, 1 (2001).
6. A. Witkiewicz-Kucharczyk, W. Bal, *Toxicol. Lett.* **162**, 29 (2006).
7. W. F. Fitzgerald, C. H. Lamborg, C. R. Hammerschmidt, *Chem. Rev.* **107**, 641 (2007).
8. T. Barkay, S. M. Miller, A. O. Summers, *FEMS Microbiol. Rev.* **27**, 355 (2003).
9. M. J. Moore, M. D. Distefano, L. D. Zydowsky, R. T. Cummings, C. T. Walsh, *Acc. Chem. Res.* **23**, 301 (1990).
10. K. E. Pitts, A. O. Summers, *Biochemistry* **41**, 10287 (2002).
11. P. Di Lello *et al.*, *Biochemistry* **43**, 8322 (2004).
12. Cys^{96}, Cys^{117}, and Cys^{159} are highly conserved in *MerB* from other sources and are essential for activity; Cys^{160} is only weakly conserved and is not essential (*10*).
13. [Tm^R] ligands have recently been effectively used to provide compounds that mimic aspects of the chemistry relevant to the active sites of sulfur-rich zinc enzymes and proteins. See, for example, (*14*).
14. G. Parkin, *Chem. Rev.* **104**, 699 (2004).
15. Abbreviations: Me = methyl, Et = ethyl, Ph = phenyl, Bu^t = *t*-butyl, R = alkyl or aryl, X = monovalent inorganic ligand, Hmim$^{Bu^t}$ = 1-*t*-butylimidazole-2-thione.
16. There is also a long-range Hg···S secondary interaction (3.3 Å) that is perpendicular to the two primary Hg-C and Hg-S bonds.
17. J. L. White, J. M. Tanski, D. Rabinovich, *J. Chem. Soc. Dalton Trans.* **2002**, 2987 (2002).
18. I. Cassidy *et al.*, *Eur. J. Inorg. Chem.* **2002**, 1235 (2002).
19. G. C. Benison *et al.*, *Biochemistry* **43**, 8333 (2004).
20. [Tm$^{Bu^t}$]HgCH$_2$CN is obtained from the reaction of [Tm$^{Bu^t}$]K, EtHgCl, and KBH_4 in MeCN.
21. C. E. Holloway, M. Melník, *J. Organomet. Chem.* **495**, 1 (1995).
22. Two-coordination at mercury is also common for thiolate compounds (*23*).
23. J. G. Wright, M. J. Natan, F. M. MacDonnell, D. M. Ralston, T. V. O'Halloran, *Prog. Inorg. Chem.* **38**, 323 (1990).
24. M. Wilhelm *et al.*, *Eur. J. Inorg. Chem.* **2004**, 2301 (2004).
25. P. Barbaro *et al.*, *Inorg. Chem.* **33**, 6163 (1994).
26. G. Gioia Lobbia, C. Santini, F. Giordano, P. Cecchi, K. Coacci, *J. Organomet. Chem.* **552**, 31 (1998).
27. Intermediate three-coordinate "T-shaped" geometries are also known. For example, the approximately linear coordination observed for [pzTp]HgMe [169(2)°] is supplemented by a secondary Hg···N interaction (*28*).
28. A. J. Canty, B. W. Skelton, A. H. White, *Aust. J. Chem.* **40**, 1609 (1987).
29. {[κ^3-N(CH$_2$CH$_2$PPh$_2$)$_3$]HgPh}$^+$ reacts with ArSH, but the reaction has been proposed to involve initial dissociation of N(CH$_2$CH$_2$PPh$_2$)$_3$ and subsequent formation of [HN(CH$_2$CH$_2$PPh$_2$)$_3$]$^+$, which is the active reagent in the protolytic cleavage, rather than the thiol (*25*).
30. Half-life ≈ 15 min for [Tm$^{Bu^t}$]HgEt with [PhSH] = 0.1 M.
31. D. Rabinovich, *Struct. Bonding* **120**, 143 (2006).
32. M. M. Kreevoy, *J. Am. Chem. Soc.* **79**, 5927 (1957).
33. Thus, whereas Me_2Hg reacts slowly with certain biologically related thiols to cleave one of the Hg-C bonds, cleavage of the second Hg-CH_3 bond could not be achieved (*34*).
34. H. Strasdeit, A. von Döllen, W. Saak, M. Wilhelm, *Angew. Chem. Int. Ed.* **39**, 784 (2000).
35. Calculations suggest that the increased facility of protolytic cleavage of the Hg-C bond upon increasing coordination number is a consequence of an associated increase in negative charge on the carbon (*36*).
36. B. Ni, J. R. Kramer, R. A. Bell, N. H. Werstiuk, *J. Phys. Chem. A* **110**, 9451 (2006).
37. See supporting material on *Science* Online.
38. The related methimazole complex [(Hmim^{Me})HgMe](NO_3) has been reported (*39*).
39. A. R. Norris, S. E. Taylor, E. Buncel, F. Bélanger-Gariépy, A. L. Beauchamp, *Can. J. Chem.* **61**, 1536 (1983).
40. The nature of the final mercury product has not been identified.
41. The positive charge on the complex could also inhibit protolytic cleavage. In this regard, the corresponding reaction of neutral [mim$^{Bu^t}$]HgR with PhSH was also investigated, but the reaction yielded PhSHgR as a result of preferential protonation of the nitrogen atom of the [mim$^{Bu^t}$] ligand. Moreover, the two-coordinate neutral compound PhSHgR is inert to excess PhSH at room temperature.
42. Addition of Hmim$^{Bu^t}$ to {[Hmim$^{Bu^t}$]HgR}$^+$ in the absence of PhSH does not result in cleavage of the Hg-C bond. Rather, the ^{1}H NMR spectrum shows that Hmim$^{Bu^t}$ merely binds reversibly, as indicated by the observation that the mercury-methyl signal for {[Hmim$^{Bu^t}$]HgMe}$^+$ shifts from δ 0.48 to 0.62 in the presence of Hmim$^{Bu^t}$.
43. Although *MerB* obtained from *E. coli* (R831b) has three cysteines at the active site, only two of these are highly conserved in *MerB* from other sources (*10*). It is therefore possible that a residue other than cysteine could also facilitate the protolytic cleavage. In this regard, studies on a model system indicate that carboxylate bases may also serve to promote protolytic cleavage of Hg-C bonds (*44*).
44. E. Gopinath, T. C. Bruice, *J. Am. Chem. Soc.* **109**, 7903 (1987).

45. Supported by NSF grant CHE-0619638, which enabled the acquisition of an x-ray diffractometer, and by NIH grant GM046502. Complete crystallographic data have been deposited in the Cambridge Crystallographic Database Centre (accession numbers 648324 to 648331).

Supporting Online Material

www.sciencemag.org/cgi/content/full/317/5835/225/DC1
SOM Text
Figs. S1 to S9
Table S1
References

26 April 2007; accepted 31 May 2007
10.1126/science.1144314

Magmatic Gas Composition Reveals the Source Depth of Slug-Driven Strombolian Explosive Activity

Mike Burton,[1]* Patrick Allard,[1,2] Filippo Muré,[1] Alessandro La Spina[1,3]

Strombolian-type eruptive activity, common at many volcanoes, consists of regular explosions driven by the bursting of gas slugs that rise faster than surrounding magma. Explosion quakes associated with this activity are usually localized at shallow depth; however, where and how slugs actually form remain poorly constrained. We used spectroscopic measurements performed during both quiescent degassing and explosions on Stromboli volcano (Italy) to demonstrate that gas slugs originate from as deep as the volcano-crust interface (~3 kilometers), where both structural discontinuities and differential bubble-rise speed can promote slug coalescence. The observed decoupling between deep slug genesis and shallow (~250-meter) explosion quakes may be a common feature of strombolian activity, determined by the geometry of plumbing systems.

Strombolian explosive activity, named after Stromboli volcano, is commonly observed on volcanoes fed by low to moderate viscosity magmas. It consists of periodic jets or explosions throwing molten lava fragments tens to hundreds of meters above open vents, which are driven by the fast up-rise of gas slugs through magma-filled conduits (*1*–*5*). It is widely agreed that gas slugs form by coalescence of smaller bubbles at depth and keep sufficient overpressure

upon ascent to disrupt their skin and the upper magma column when they burst at the surface. However, both the depth at which slugs form and the mechanism of slug coalescence—be it differential bubble-rise rate in conduits (*2*, *3*) or bubble foam accumulation at structural discontinuities (*4*, *5*)—remain poorly constrained. Shallow source depths for strombolian explosions are estimated from associated seismic (*6*–*10*) and acoustic (*9*–*12*) signals, but whether these coincide with the slug source depth is unknown.

We provide quantitative constraints for the depth of slug genesis producing strombolian activity, based on spectroscopic measurements of the magmatic gas phase driving explosions at Stromboli volcano. Stromboli island, in the Aeolian archipelago, is the emerged upper part of a ~3-km-high stratovolcano erupting a volatile-rich high-potassium (HK) arc basalt (*13*–*15*). Its standard activity consists of quiescent magma degassing through crater vents located at 750 m above sea level and brief (10- to 15-s) explosions that, every 10 to 20 min, launch crystal-rich scoriae and lava blocks to 100- to 200-m height. According to geophysical signals (*6*–*8*, *11*, *12*), these periodic explosions originate at shallow depth (~250 m) below the vents. Although spectacular, they contribute little of the bulk volatile discharge, most of which is supplied by quiescent degassing (*16*, *17*). Episodically, the volcano also produces more powerful, deeper-derived explosions (*14*, *18*) that have no clear warning signal [apart from recent observations of precursory changes in gas composition (*19*)] and constitute a major hazard for the thousands of visitors and volcanologists alike. Therefore, improved understanding of the processes controlling the different types of explosions at Stromboli is also a high priority for civil defense.

Between mid-2000 and September 2002, we repeatedly measured the chemical composition of Stromboli magmatic gases between and during explosions, using open-path Fourier transform infrared (OP-FTIR) spectroscopy. With this remote sensing tool, recently used by volcanologists (*20*–*23*), magmatic gases issuing from the crater vents could be analyzed from a safe distance and with high temporal resolution (~4-s period). Here, we present and discuss one representative data set obtained on 9 April 2002, during 3.2 hours of passive and explosive degassing at the southwest vent that was most active at the time. Our spectrometer overlooked this vent from a slant distance of 240 m. We acquired double-sided interferograms, which we subsequently Fourier transformed, using the infrared radiation emitted from the hot crater floor and/or molten lava ejecta. The obtained FTIR absorption spectra allowed simultaneous retrieval of the path amounts (in molecules cm^{-2}) of major volcanic gas species (H_2O, CO_2, SO_2, and HCl) and minor volcanic gas species (CO and COS), with an accuracy ranging from ±4 to 6% for the purely volcanic species to, respectively, ±10% and 20 to 25% for CO_2 and H_2O, the amounts of which had to be corrected for air background (*22*). Details of the operating conditions and data retrieval procedures are given in (*24*).

The observed variations in radiating source temperature, volcanic gas amounts (Fig. 1), and derived molar gas compositions (Table 1) revealed the following features: (i) Quiescent gas release between the explosions has a well-defined, quite steady mean composition. It contains ~83 mol % of water vapor; it has mean CO_2/SO_2 and SO_2/HCl ratios of ~8 and 1.0 to 1.5, respectively; and according to its CO/CO_2 ratio, it last equilibrates at 630° to 760°C even though it was at close-to-ambient temperature (17° to 30°C) when measured. (ii) Each explosion is marked by sharp increases in the IR source temperature and the volcanic gas temperature and amounts. At the very onset of an explosion, the gas is as hot as the radiating ejecta (up to 970°C),

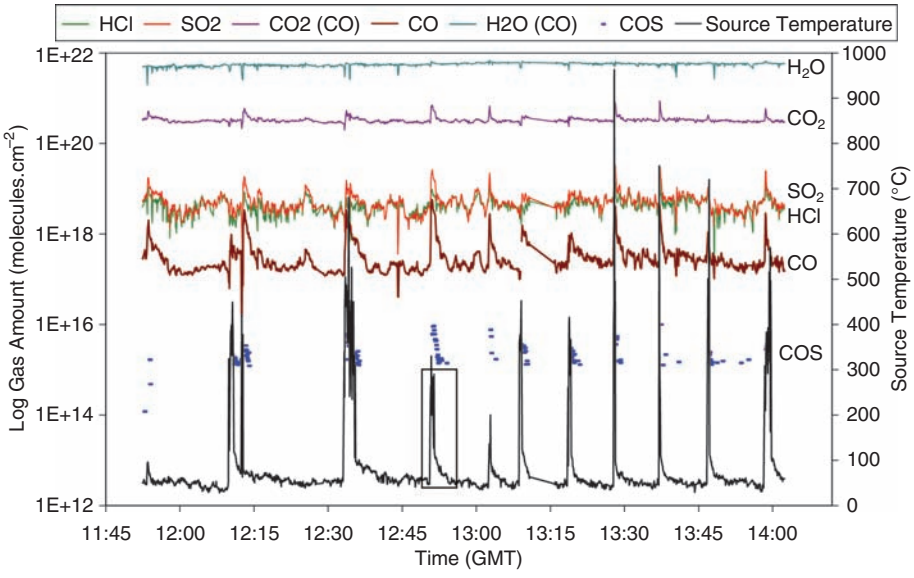

Fig. 1. Time series of volcanic gas amounts (molecules cm^{-2}) and radiating source temperature measured during quiescent and explosive degassing on Stromboli (9 April 2002). Quiescent emissions produce a background composition over which sharp bursts of gas, enriched in CO_2, SO_2, CO, and COS, are measured during explosions. These bursts coincide with peaks in radiation source temperature due to the ejection of molten lava clots. The third explosion, whose gas composition is reported in Table 1, is boxed and shown in greater detail in fig. S1.

Table 1. Molar gas compositions during quiescent and explosive crater degassing at Stromboli volcano, measured with OP-FTIR spectroscopy. "Typical explosion" shows the gas composition during the explosion shown in Fig. 2 and the average gas ratios (±1σ) for similar such explosions. "Smaller explosions" shows the average gas composition for smaller, CO_2-poorer explosions. The equilibrium gas temperatures (Equil. temp.) were computed from measured CO/CO_2 ratios and thermodynamic data for the reaction $2CO + O_2 = 2CO_2$, assuming ideal gas behavior and redox buffering by Stromboli basalt [$\log fO_2$ ~ NNO + 0.3 (*34*); NNO, nickel-nickel oxide buffer]. Source pressures were inferred from the modeled degassing of Stromboli basalt during decompression (Fig. 3). b.d., below detection limit.

Gas features	Quiescent degassing	Typical explosion	Smaller explosions
H_2O %	82.9	64.4	79.3
CO_2 %	13.6	33.1	19.0
SO_2 %	1.7	1.8	1.15
HCl %	1.7	0.33	0.43
CO %	0.03	0.44	0.15
COS %	b.d.	0.008	b.d.
H_2O/CO_2	6.1	2.3 ± 0.8	4.5 ± 2.3
CO_2/S	7.8	20.7 ± 2.1	16.8 ± 1.9
S/Cl	1.0–1.5	4.7 ± 0.8	2.5 ± 0.8
CO/SO_2 (10^{-2})	1.8	24.0 ± 0.9	14.6 ± 0.4
CO/CO_2 (10^{-2})	0.21	1.14 ± 0.09	0.9 ± 0.08
Equil. temp. (°C)	700	1020–1130	1000–1060
Source pressure (MPa)	≤0.3–4	~70–80	~20–50

[1]Istituto Nazionale di Geofisica e Vulcanologia, Catania, Italy. [2]Groupe des Sciences de la Terre, Laboratoire Pierre Süe, CNRS-CEA, Gif-sur-Yvette, France. [3]Dipartimento di Chimica e Fisica della Terra ed Applicazioni, Palermo University, Palermo, Italy.

*To whom correspondence should be addressed. E-mail: burton@ct.ingv.it

which prevents its analysis. Sudden expansion of the eruptive cloud produces an apparent drop in background gas amounts (Fig. 1), due to shorter beam path length. After a few seconds, however, the explosive gas phase rapidly cools through expansion and air dilution, whereas the radiation source (fresh lava clots on the crater floor) cools more slowly, providing a large temperature contrast and simple absorption spectra. Subtracting the background gas amount measured immediately before each explosion from the amount produced by the explosion allowed us to determine the chemical composition of the pure slug gas. Once cooled enough, the latter displays a stable composition (Fig. 2) that can be observed for a minute or so before the eruptive cloud gradually dissipates. We find that the slug gas markedly differs from the quiescent emissions: It is less hydrous, richer in CO_2, SO_2, CO, and COS, and its CO_2/SO_2, SO_2/HCl, and CO/CO_2 ratios are three to five times as high. Moreover, its computed equilibrium temperature (1000° to 1140°C) closely matches that of the molten basalt (Table 1). Therefore, the gas phase driving the explosions preserves the memory of hotter but also deeper source conditions, as shown by its enrichment in early exsolving volatile species such as CO_2.

Similar observations made for explosions at different periods suggest a reproducible source process. However, the explosions separated by "standard" repose intervals of ~15 to 20 min (such as the second to fifth peaks in Fig. 1) were generally found to display more reproducible and higher CO_2/SO_2, CO/SO_2, and SO_2/HCl ratios but a lower H_2O/CO_2 ratio than smaller explosions succeeding at shorter intervals (Table 1). Accordingly, the smaller explosions may have a more shallow origin, consistent with their higher frequency and lower energy, or they may be powered by smaller and hence slower slugs that suffer greater contamination by gas—present in the shallow conduit—that is poor in CO_2-S and richer in Cl-H_2O.

Melt inclusion studies of volatiles dissolved in Stromboli HK-basalt (*11*–*13*) provide the key information to interpret our results. Primitive inclusions of the basaltic melt entrapped in olivine at about 280 MPa (~10-km depth) contain on average 3.0 weight (wt) % H_2O, 0.12 wt % CO_2, and 0.17 wt % of S and Cl (*13*–*15*). At that pressure, the basalt already coexists with ~2.5 wt % of CO_2-rich gas formed by early exsolution of the abundant CO_2 contained in Stromboli parental magma (*25*). Starting from these data and using the VolatileCalc software (*26*), we computed the pressure-related evolution of H_2O and CO_2 in the melt and the gas phase during closed-system ascent and differentiation (tracked by K_2O) of the HK-basalt from 280 MPa to the surface. The amounts of S and Cl degassed during this process were then estimated from the best fit of their dissolved content with respect to H_2O and K_2O in melt inclusions (*13*–*15*). The main sources of uncertainty in our modeling arose from the sparse number of melt inclusions recording intermediate pressures and, to a lesser degree, from intrinsic limitations of VolatileCalc in simulating the degassing of water-rich basalt (*26*). Notwithstanding these issues, the modeled degassing trends reproduced fairly well both petrologic observations and the FTIR-measured gas compositions. Figure 3 shows the variations of H_2O/CO_2, CO_2/S, and S/Cl molar ratios in the equilibrium gas phase as a function of pressure between 100 and 0.1 MPa [S and Cl here refer to the exsolved amounts of bulk elemental sulfur and chlorine which, in surface emissions, predominantly occur as SO_2 and HCl, as shown here and in (*16*, *17*)].

We highlight two conclusions. (i) The chemical composition of quiescent emissions is well reproduced by complete degassing of the uprising basalt, with a transition from closed- to open-system conditions in the shallow volcanic conduits. This is consistent with a steady-state process of magma ascent, degassing, and convective overturn that contributes the bulk of the volcanic gas output (*16*, *17*). The emitted gas only diverges from the modeled composition in its higher water content and slightly lower S/Cl ratio (Table 1 and Fig. 3). We attribute these discrepancies to both spectroscopic interferences from low-temperature, water- and Cl-rich crater rim fumaroles (*27*, *28*) and probable entrainment of meteoric steam from the shallow hydrothermal system. (ii) The gas slugs driving Strombolian explosions cannot have a shallow origin. Instead, their measured compositions correspond to those achieved by the equilibrium gas phase under confining pressures of ~70 to 80 MPa (most energetic explosions) to ~20 MPa (smallest explosions). To preserve these compositions at the surface, the slugs must then rise separately from the magma from depths between ~2.7 and

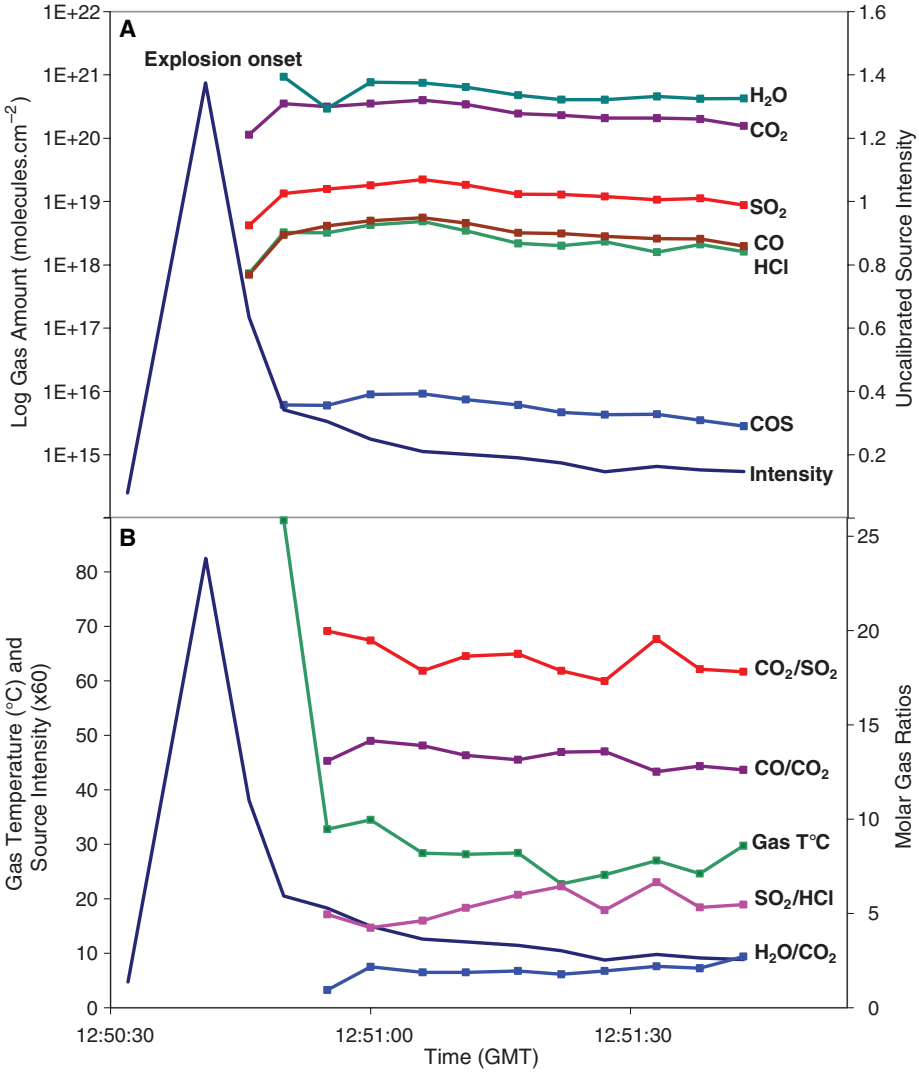

Fig. 2. (**A**) Gas amounts and (**B**) molar gas ratios of the pure slug phase driving one illustrative Strombolian explosion (which occurred at 12:50:41 GMT). At the explosion onset, marked by a peak in radiative intensity, the gas is as hot as the radiation source, preventing detection. As the gas cools, the thermal contrast between the radiation source (molten lava clots) and the gas increases until its stable composition is observed.

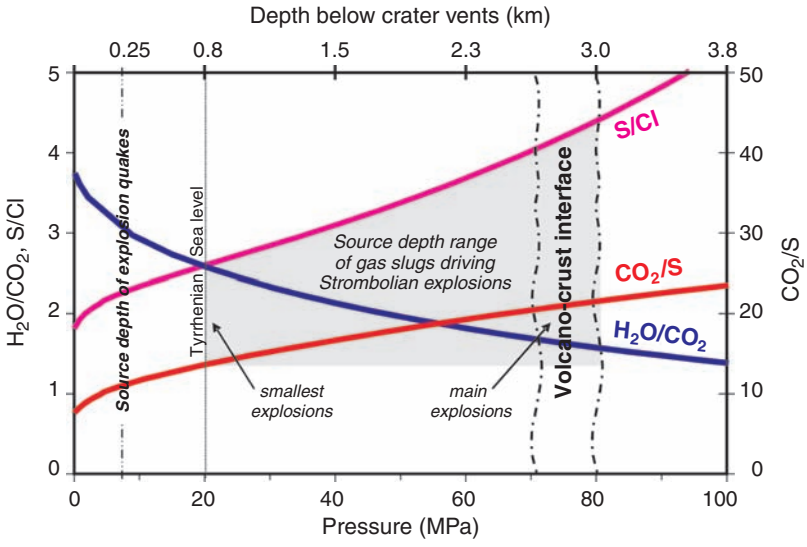

Fig. 3. Pressure-related modeled evolution of H_2O/CO_2, CO_2/S, and S/Cl molar ratios in the magmatic gas phase during closed-system ascent, differentiation, and degassing of Stromboli HK-basalt (100 to 0.1 MPa) and inferred source depths of gas slugs driving Strombolian explosions. Gas modeling was performed using (i) the chemistry and dissolved volatile content of olivine-hosted melt inclusions representative of the primitive and evolved basalt (*13*–*15*); (ii) the original CO_2 content of Stromboli parental magma (*25*); and (iii) VolatileCalc software (*26*). The VolatileCalc software was used to compute the step-by-step evolution of H_2O and CO_2 in the melt and the gas phase from initial boundary conditions of P = 280 MPa, T = 1140°C, and melt SiO_2 = 48.5 wt %. Partial sulfur exsolution during genesis of Stromboli HK-basalt (*13*) has been taken into account. The measured CO_2/S and S/Cl ratios of gas slugs driving Strombolian explosions require their separate ascent from pressures of ~80 to 70 MPa to 20 MPa, or ~3- to 0.8-km depth below the vents (i.e., from between the volcano-crust interface and the Tyrrhenian Sea level). This is much deeper than the source depth (~250 m) of explosion quakes (*6*–*8*). H_2O/CO_2 ratios suggest somewhat lower but more uncertain source depths, owing to larger analytical uncertainty on emitted H_2O and probable entrainment of hydrothermal meteoric steam during shallow slug ascent.

0.8 km below the vents (for a rock density of 2700 kg m^{-3})—that is, from between about the base of the volcanic pile and the Tyrrhenian Sea level (Fig. 3). In that depth interval, the melt vesicularity increases rapidly from ~0.35 to ~0.7, promoting a transition from closed- to open-system degassing (*29*). At the volcano-crust interface, slug genesis could thus result either from bubble accumulation and foam growth at structural discontinuities (*4*, *5*) or from the coalescence of bubbles with different sizes and rise speeds (*2*, *3*). Discriminating between these two processes is challenging, even though the former should be favored by increased flow rate of gas-rich magma and could thus explain increases in tremor (*30*), explosion-quake frequency, and gas flux (*31*) that are observed during periods of elevated activity. Increasing magma permeability in the shallow volcanic conduits would rather inhibit slug coalescence. Therefore, unless another geometrical discontinuity exists at ~1 km below the vents, the most shallow gas compositions associated with the weakest explosions may reflect greater incorporation of shallow bubbles into slowly rising, smaller slugs, which formed at the volcano-crust interface.

We demonstrate here that Stromboli's recurrent explosions have much deeper roots than previously inferred from geophysical data (*6*–*8*, *11*, *12*). The shallow (~250-m) source depth of explosion quakes and associated acoustic signals do not signify a shallow origin of the rising gas slugs. Instead, these signals are the result of a permanent structural discontinuity at the base of the upper conduits, where deeper-derived gas slugs undergo an abrupt flow-pattern change (*32*) before bursting at the surface. This conclusion is supported by the unchanged source location of explosion quakes during the 2002-2003 lava flow eruption (*31*), despite lateral drainage of the upper magma column. We thus reveal a strong decoupling between geophysical signals of the explosions, controlled by structural discontinuity, and the true process of slug genesis. Such an observation may apply to several other volcanoes (such as Villarica, Erebus, Masaya, Yasur, and Arenal) displaying comparable persistent explosive activity, depending on their magma volatile content and the geometry of their plumbing system. Recent FTIR measurements on Yasur (*23*) detected weak CO_2 enrichment of gas driving explosions, but the lack of constraints from seismic or petrological data prevented quantitative assessment of the slug source depth. Improved understanding of the mechanisms controlling strombolian explosive activity clearly requires multidisciplinary investigations. As shown here, spectroscopic measurement of the driving magmatic gas phases is a powerful tool in such studies.

References and Notes

1. R. S. J. Sparks, *J. Volcanol. Geotherm. Res.* **3**, 1 (1978).
2. L. Wilson, J. W. Head III, *J. Geophys. Res.* **86**, 2971 (1981).
3. E. A. Parfitt, *J. Volcanol. Geotherm. Res.* **134**, 77 (2004).
4. C. Jaupart, S. Vergniolle, *Nature* **331**, 58 (1988).
5. C. Jaupart, S. Vergniolle, *J. Fluid Mech.* **203**, 347 (1989).
6. B. Chouet *et al.*, *J. Geophys. Res.* **102**, 15129 (1997).
7. B. Chouet *et al.*, *J. Geophys. Res.* **108**, 2019 (2003).
8. M. Ripepe, S. Diliberto, M. D. Schiava, *J. Geophys. Res.* **106**, 8713 (2001).
9. C. A. Rowe, R. C. Aster, P. R. Kyle, R. R. Dibble, J. W. Schlue, *J. Volcanol. Geotherm. Res.* **101**, 105 (2000).
10. M. T. Hagerty, M. Protti, S. Y. Schwartz, M. A. Garces, *J. Volcanol. Geotherm. Res.* **101**, 27 (2000).
11. S. Vergniolle, G. Brandeis, J.-C. Marechal, *J. Geophys. Res.* **101**, 20449 (1996).
12. M. Ripepe, A. J. L. Harris, R. Carniel, *J. Volcanol. Geotherm. Res.* **118**, 285 (2002).
13. N. Métrich, A. Bertagnini, P. Landi, M. Rosi, *J. Petrol.* **42**, 1471 (2001).
14. A. Bertagnini, N. Métrich, P. Landi, M. Rosi, *J. Geophys. Res.* **108**, 2336 (2003).
15. P. Landi, N. Métrich, A. Bertagnini, M. Rosi, *Contrib. Mineral. Petrol.* **147**, 213 (2004).
16. P. Allard, J. Carbonnelle, N. Métrich, H. Loyer, P. Zettwoog, *Nature* **368**, 326 (1994).
17. P. Allard *et al.*, *Geophys. Res. Lett.* **27**, 1207 (2000).
18. F. Barberi, M. Rosi, A. Sodi, *Acta Vulcanol.* **3**, 173 (1993).
19. A. Aiuppa, C. Federico, *Geophys. Res. Lett.* **31**, L14607 (2004).
20. T. Mori *et al.*, *Earth Plan. Sci. Lett.* **134**, 219 (1995).
21. P. W. Francis, M. Burton, C. Oppenheimer, *Nature* **396**, 567 (1998).
22. P. Allard, M. Burton, F. Muré, *Nature* **433**, 407 (2005).
23. C. Oppenheimer, P. Bani, J. Calkins, M. Burton, G. M. Sawyer, *Appl. Phys. B* **85**, 453 (2006).
24. Data were collected with a Bruker OPAG-22 FTIR spectrometer, working at 0.5 cm^{-1} resolution. Single-scan, double-sided interferograms were collected every ~4 s and were Fourier transformed offline with the use of Norton-Beer medium apodization. Spectral analysis was performed with a nonlinear least-squares fitting program and an adapted forward model based around the Reference Forward Model (*33*). The different physical conditions of atmospheric and volcanic gases were taken in account using a two-layer atmospheric model. Volcanic gas temperature was retrieved by fitting this parameter during analysis of the SO_2 $\nu_1 + \nu_3$ combination band at 2500 cm^{-1}, whose rotational line envelope is highly temperature dependent. Source temperatures were determined from the ratio of the observed signal at 4400 and 4460 cm^{-1} and fitting to a Planck curve. Quiescent degassing compositions between the explosions were determined with the use of linear fits to correlation plots of volcanic gas amounts.
25. P. Allard, abstract GMPV7-8044, presented at the European Geophysical Union General Assembly, Vienna, Austria, 16 to 20 April 2007.
26. S. Newman, J. B. Lowenstern, *Comput. Geosci.* **28**, 597 (2002).
27. M. Chaigneau, *C. R. Acad. Sci. Paris* **261**, 2241 (1965).
28. M. L. Carapezza, C. Federico, *J. Volcanol. Geotherm. Res.* **95**, 227 (2000).
29. M. Burton, H. Mader, M. Polacci, P. Allard, *Eos* **86** (Fall Meeting Suppl.), 52 (abstr. V13G-01) (2005).
30. H. Langer, S. Falsaperla, *Pure Appl. Geophys.* **147**, 57 (1996).
31. M. Ripepe *et al.*, *Geology* **33**, 273 (2005).
32. M. R. James, S. J. Lane, B. A. Chouet, *J. Geophys. Res.* **111**, B05201 (2006).
33. A. Dudhia, University of Oxford, www.atm.ox.ac.uk/RFM.
34. N. Métrich, R. Clocchiatti, *Geochim. Cosmochim. Acta* **60**, 4151 (1996).

35. We gratefully acknowledge the Dipartimento di Protezione Civile of Italy for helicopter support that proved essential for OP-FTIR measurements on Stromboli and for support via project V2: Stromboli. We thank A. Bonaccorso, S. Calvari, and E. Boschi for their continuous support and N. Métrich (LPS, Saclay, France) for helpful discussions on melt inclusion data.

Supporting Online Material

www.sciencemag.org/cgi/content/full/317/5835/227/DC1
Fig. S1

28 February 2007; accepted 16 May 2007
10.1126/science.1141900